Numerical Simulation of Storm Surges and Waves Caused by Typhoon Jebi in Osaka Bay with Consideration of Sudden Change of Wind Field

*Kazuhiro TANAKA, **Masaki WASHIDA, ***Yoshihiro NISHIUKE,
****Tetsuya HIRAISHI

* Coastal & Ocean-front Department, Coastal & Ocean-front Division, Japan Port Consultants, Ltd.
** Engineering Department, Osaka Branch, Central Consultant Inc.
*** System Development Department, Aquatic Zone Network Co., Ltd.
**** Disaster Prevention Research Institute (DPRI), Kyoto University

Abstract

Typhoon Jebi (T1821) was a high-speed typhoon with a moving speed exceeding 60 km/h at landfall, and with a further acceleration of the moving speed just before 14:00 on September 4, 2018, formed an extremely strong wind field, causing a storm surge and high wave disasters along the northern coast of Osaka Bay.

This study conducted a numerical simulation of storm surges and waves using the wave-surge combined numerical model taking the effects of moving speed acceleration into consideration by enhancing the JMA GPV wind data. The computation successfully reproduced the disaster external forces in Kobe and Osaka Ports, Yodo River mouth, and Kansai International Airport. The major findings of the study are summarized as follows:

(1) Numerical analysis considering the rapid increase of surface wind due to acceleration of the typhoon moving speed reproduced the storm surge anomaly exceeding 2.77 m observed at the northern end of Osaka Bay.

(2) The storm surge water level in Yodo River exceeding O.P.+5.2 m was also reproduced.

(3) The computed total water level was CDL+4.16 m (storm surge + wave run-up height + margin height) on the southeast side of Kansai International Airport Island that exceeded the current crown height of CDL+3.9 m.

KEY WORDS : Typhoon Jebi (T1821), storm surge and high wave disaster, SWAN, POM, wave breaking stress, radiation stress gradient

1. INTRODUCTION

In 2018 Typhoon Jebi (T1821) passed the west side of the Kii Channel and Osaka Bay at a high speed of 60 to 65 km/h while maintaining a strong central pressure of 950 hPa, and after further acceleration from the northern end of Osaka Bay entered the Sea of Japan with an average moving speed of more than 93 km/h. The wind speed increased rapidly due to the acceleration of the typhoon moving speed, and the strong winds occurred when the wind direction changed from east to south between 13:00 and 14:00 on September 4, 2018. On Kansai Airport Island, a ferocious wind was recorded, and the maximum instantaneous wind speed was 58.1 m/s at 13:38 and the 10-minute average wind speed was 46.5 m/s at 13:47 (Japan Meteorological Agency: JMA (2018)). Since the central pressure of the typhoon at landfall was as low as 950 hPa, in addition to the suction effect of more than 0.5 m, the rapid increase in moving speed just before 14:00 emphasized the drifting effect in the shallow waters, and maximum storm surge anomalies of 2.77 m in the Port of Osaka and 1.81 m in the Port of Kobe were recorded. In addition, it overlapped with the lower high tide level of diurnal inequality of Tokyo Pail (T.P.) +0.32 m as shown in Figure 1, and recorded a high tide level of 3.29 m at 14:18 Japan

Standard Time (JST) in the Port of Osaka and a high tide of 2.33 m at 14:09 JST in the Port of Kobe.
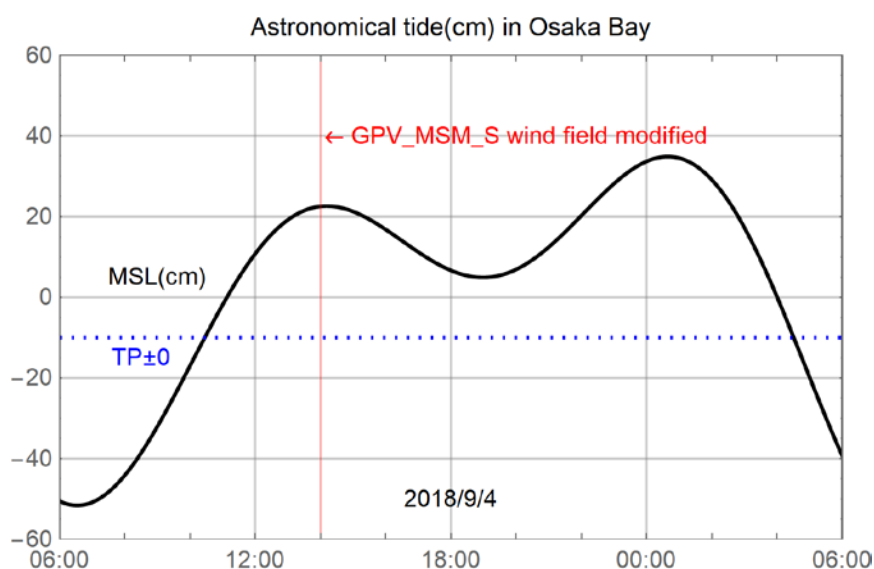
Fig. 1. Astronomical tide on September 4th, 2018 and the relation between
Mean Sea Level (MSL) and Tokyo Pail (T.P.) in Osaka Bay.

To prevent coastal disasters, it is necessary to clarify the relationship between the design crown height of coastal embankments and the maximum significant wave height and storm surge anomaly caused by the typhoon. The design crown height is defined as the design storm surge height + wave run-up height + margin height. The design storm surge height is defined as the average syzygy high tide level (T.P.+0.9 m in Osaka Bay) + estimated storm surge anomaly. Assuming that the wave run-up height is half of the wave height, the design storm surge height in Osaka Bay is estimated as T.P.+4.9 m in the region where the wave height is 2.0 m and the estimated storm surge anomaly is 3.0 m. The occurrence of storm surge and high wave disasters due to overtopping and overflowing is expected in many reclamation areas where the design crown height was set at less than T.P.+4.9 m. In reality, immense damage occurred mainly in the reclamation area along the coast of Osaka Bay, such as inundation of runways at Kansai International Airport (KIX) and inundation and container outflows in many artificial islands.

After the typhoon passed, a numerical simulation of storm surges and high waves along the coast of Osaka Bay was conducted using meteorological reanalysis data (the surface winds and atmospheric pressure) of the Japan Meteorological Agency (JMA)'s Grid Point Value (GPV) hourly data, and it was revealed that the computational results were underestimated.

To consider the effects of rapid increase in the wind speed associated with the movement of a typhoon, we modified the wind speed field between 13:00 and 14:00, September, 4th. We reproduced storm surges and waves in Osaka Bay by using the modified wind field. Using the simulation output, we discuss the temporal and spatial distribution of external forces of storm surge disasters that occurred in Hanshin Port, the Yodo River channel, and Kansai International Airport Island.

2. ANALYSIS METHOD

2.1 Numerical model framework
Storm surges occur due to the formation of static sea level gradients due to atmospheric pressure gradients and the water level rise caused by the dynamic flow driven by wind and waves being stopped at the shore (drifting effect). The former is called the suction effect, and the latter flow formation mechanism is classified into offshore wind-driven flow and nearshore current with wave

setup in the coastal zone due to surf zone wave breaking. As for the suction effect, a water level rise of about 1 cm occurs with a pressure drop of 1 hPa regardless of the water depth. The drifting effect is only flow formation in the deep sea, but in shallow water, the increased flow velocity is blocked by the shore and a sudden rise in water level occurs. Furthermore, the mean sea level rise (wave setup) is also generated by the breaking wave (surf zone wave breaking) where the energy carried by the wave is transferred to nearshore currents and wave setup. Most atmospheric energy contributes to the generation and development of wind waves due to wind shear stress acting on the ocean surface. The offshore white-cap breaking phenomenon (white capping) generates mean ocean currents and turbulence, and the energy propagated as waves generates large-scale turbulences and nearshore currents with wave setup in the surf zone.

Based on this understanding, we established the numerical model combining the third-generation shallow water wave model, SWAN Cycle III Version 41.01 (2014) and the current Princeton Ocean Model (POM) of ECOMSED (version 1.3) that is the three-dimensional hydrodynamic module, ECOM, developed by Blumberg and Mellor (1980, 1987). For the nesting computation, we adopted the method of surface water level communication from the mother domain to the next domain. In this calculation, we used GPV_MSM_S data (surface pressure and wind speed) of the JMA as the meteorological field. As the driving force of the flow, we adopted the concept of breaker stress, and defined wave breaking stress in which the wave energy lost by whitecap wave breaking and surf zone breaking functioned as surface shear stress in the direction of energy propagation at group velocity.

Wave energy was transferred to both the mean current and turbulence. In this energy transfer ratio of mean current and turbulence, meaning the mean current generation efficiency, we assumed that the whitecap breaking has an efficiency of 0.9 and the surf zone breaking has 0.66. As the same analysis method, it is possible to estimate the driving force via the radiation stress gradient, but when using a rough grid system of wave simulation, there is a limit to the spatial resolution of the gradient, which is not efficient. The model structure of the wind-wave-current relation and the used surface stresses are shown in Figure 2.
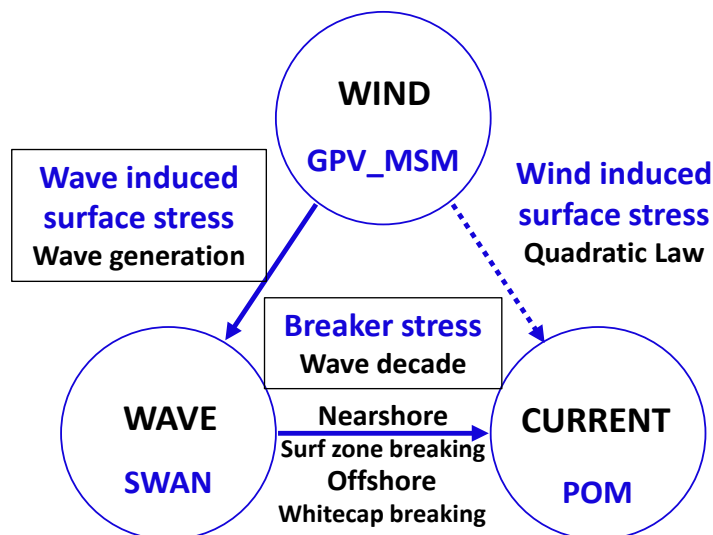
Fig. 2. Model structure of wind-wave-current relation and used surface stresses.

2.2 Driving forces of storm surge generation

When the coastal ocean current is computed combined with wave analysis, the surface stress of the ocean current can be estimated by breaking wave stress or radiation stress gradient. The outline of the driving force that generates storm surge (external force of ocean current generation) is shown below.
(1) Wave breaking stresses:
     Most of the surface wind energy is used for the formation of waves, and the developed wave

energy shifts to currents (average flow and turbulence) through wave breaking. In order to describe this process, we propose the wave breaking stress defined by Eq. (1), in which the driving force of the ocean current generation is described using energy transfer from the wave energy dissipation rates to ocean currents through both of the whitecap breaking and the surf zone wave breaking.

$$\tau_{break} = \varepsilon_w \frac{S_{wcap}}{c_g} + \varepsilon_s \frac{S_{surf}}{c_g} \tag{1}$$

where, S_{surf} is the energy dissipation rate due to surf zone breaking (in W/m^2), S_{wcap} is the energy dissipation rate due to white capping (in W/m^2), and c_g is the group velocity. For TDIR in SWAN output, the direction of energy transport is used to set the tensor in x (east is positive) and y (north is positive) directions.

For the formulation of the surf zone breaking (the energy dissipation in random waves due to depth-induced breaking), the bore-based model of Battjes and Janssen (1978) is used in the wave model of SWAN. In this computation, third-generation physics GEN3 of Westhuysen was employed, so the formulation of whitecap dissipation is the nonlinear saturation-based white capping combined with wind input (Yan, 1987).

The efficiency, ε_w, and ε_s, in Eq. (1) can be considered as the energy ratios of the generated current and turbulence, through white capping and surf zone breaking, respectively. In this computation, we set $\varepsilon_w = 0.9$ and $\varepsilon_s = 0.66$.

(2) Radiation stress gradient:

Wave-induced forces per unit surface area, F_x and F_y (N/m^2), are formulated by the gradient of the radiation stress tensor as follows:

$$F_x = -\frac{\partial S_{xx}}{\partial x} - \frac{\partial S_{xy}}{\partial y}, \ F_y = -\frac{\partial S_{yx}}{\partial x} - \frac{\partial S_{yy}}{\partial y} \tag{2}$$

where, using the energy density, E, the water density, ρ, the gravity acceleration, g, wave propagation angle, θ, and angular frequency, σ, the radiation stress tensors are given as:

$$S_{xx} = \rho g \int \left(c_g \cos^2 \theta + c_g - \frac{1}{2} \right) E d\sigma d\theta \tag{3}$$

$$S_{xy} = S_{yx} = \rho g \int (c_g \sin \theta \cos \theta) E d\sigma d\theta \tag{4}$$

$$S_{yy} = \rho g \int \left(c_g \sin^2 \theta + c_g - \frac{1}{2} \right) E d\sigma d\theta \tag{5}$$

(3) Wind stress (quadratic law of wind speed)

When estimating sea surface shear stress from only wind speed information, the quadratic law is frequently employed. Equation (6) is the wind stress formulation used in POM of ECOMSED.

$$\tau_{surface} = \rho_a C_D \vec{W} |\vec{W}| \tag{6}$$

$$C_D = \begin{cases} 1.2 \times 10^{-3} & (|\vec{W}| < 11) \\ (0.49 + 0.065 * |\vec{W}|) \times 10^{-3} & (25 > |\vec{W}| \geq 11) \\ (0.49 + 0.065 * 25) \times 10^{-3} & (|\vec{W}| \geq 25) \end{cases} \tag{7}$$

Figure 3 shows a snapshot of the spatial distribution of (a) wave breaking stress, (b) wind stress of 1.83 times quadratic law, and (c) radiation stress gradient. Strong stresses appear in the coastal area in the Kii Channel for the wave breaking stress and the radiation stress gradient. This is

due to wave breaking in the surf zone. The offshore radiation stress gradient is clearly smaller than the cases of wind stress and wave breaking stress. This indicates that the radiation stress gradient cannot be used as the driving force for the ocean current generated in the offshore region. From our experience of past storm surge analysis, the wind stress of Eq. (6) should be enhanced by multiplying the factor of 1.83 to reproduce the observed surge heights. This plane distribution almost corresponds to that of the wave breaking stress evaluated by Eq. (1). This indicates that the sea surface stress obtained by Eq. (6) is being underestimated. Actually, the computed storm surge by the surface stress of Eq. (6) is quite small, and the enhanced wind stress can reproduce the observed storm surge height.


(a) Wave breaking stress

(b) Wind stress (1.83 times of quadratic law)

(c) Radiation stress gradient
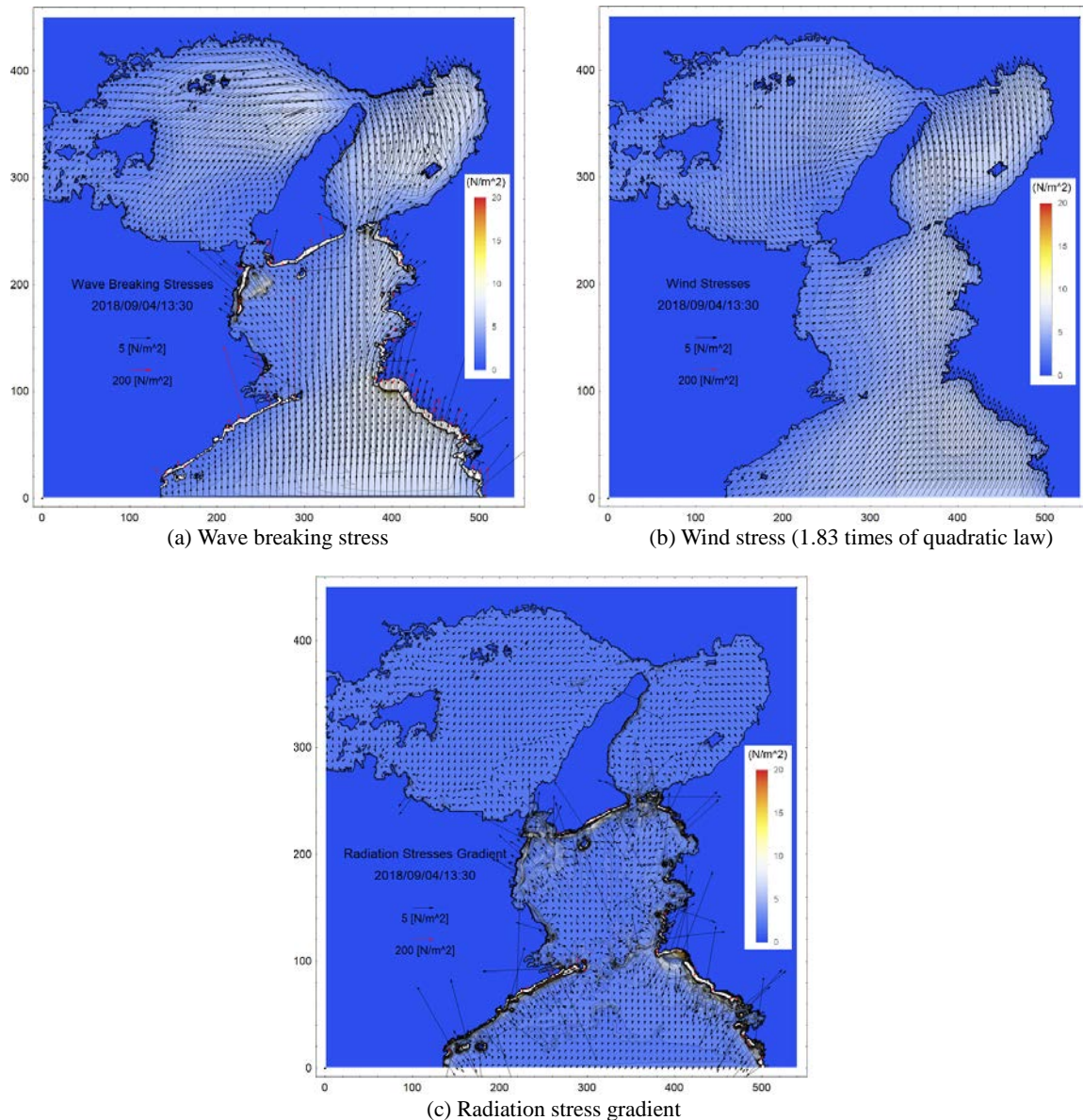
Fig. 3. Snapshot of surface forces by three types of surface shear stress formulations.

2.3 Computational domain and procedure

Since the three areas of Osaka Bay, Harimanada Sea, and Kii Channel are connected by straits, the resonance characteristics of ocean oscillation in each area need to be analyzed simultaneously as a cooperative system. Since the Kii Strait is connected to the Pacific Ocean, the boundary conditions of ocean waves and tides are given at the southern end of this area.
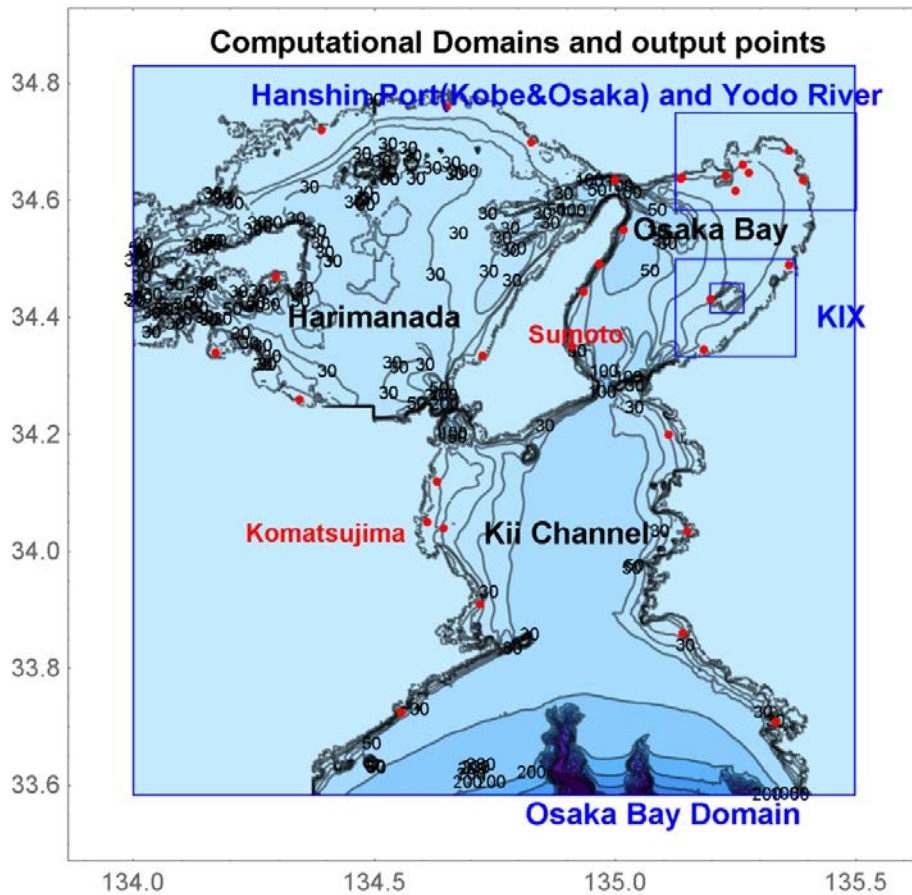
Fig. 4. Ocean depth and output points of the computational domains of Osaka Bay, and the nested domains of KIX, Hanshin Ports (Kobe and Osaka), and Yodo River.

In this analysis, the computational domain was a combination of three sea areas as shown in Figure 4. The larger computational domain is Osaka Bay Domain, which is an orthogonal lattice network with a spatial resolution of 0.002778 degree (hereinafter called "250 m mesh"). Two nesting domains were set for the area of Hanshin Port, Yodo River estuary and the Kansai International Airport Island. The former is a nesting domain of a 0.000556 degree (hereinafter called "50 m mesh") mesh for the Port of Kobe, Port of Osaka, and Yodo River estuary and lower channel. The latter is a nesting domain with a 50 m mesh area surrounding the sea of Kansai International Airport and a "10 m mesh" (0.000111 degree) around the airport island to reproduce storm surges in the river channel and possible storm surge occurrence around the airport island.

Ocean and coastal topography was reproduced by the datasets of M7014 and M7010 of the M7000 series nautical chart provided the Japan Hydrograph Association. The coastal lines are set by the "10 m mesh" DEM of the national land base map. The reference plane of the nautical chart is the lowest depth of chart reference (Chart D.L.), which coincides with the reference plane of Osaka Pail (O.P.). The detailed topography in the Hanshin Port area was not taken into account because of lack of data in the M7000 series nautical chart. A uniform water depth of 8.85 m from MSL was assumed. In the lower part of the Yodo River, the average depth of O.P.+5.0 m of the standard river profile data was used, where O.P. is 1.3 m lower than Tokyo Pail (T.P.), O.P. = T.P.+1.3 m.

3. TYPHOON JEBI AND ITS WIND FIELD MODIFICATION

3.1 Typhoon track and moving speed

Figure 5 shows the position of Typhoon Jebi, the isobar near the center, the moving speed, and the central pressure every hour. The blue lines in the figure indicate the domains for storm surge and wave computations. This figure shows that Typhoon Jebi landed in Tokushima Prefecture at 11:00, then moved north at a moving speed of 60-64 km/h, and landed again in Hyogo prefecture around 14:00. After arriving in Hyogo prefecture, the moving speed increased rapidly, and the typhoon moved out to the Sea of Japan at an average speed of 93 km/h. The moving speed of the typhoon increased sharply by about 1.5 times, and the moving wind speed is thought to have increased on the right side of the typhoon path. On the left side, the wind speed slowed down.
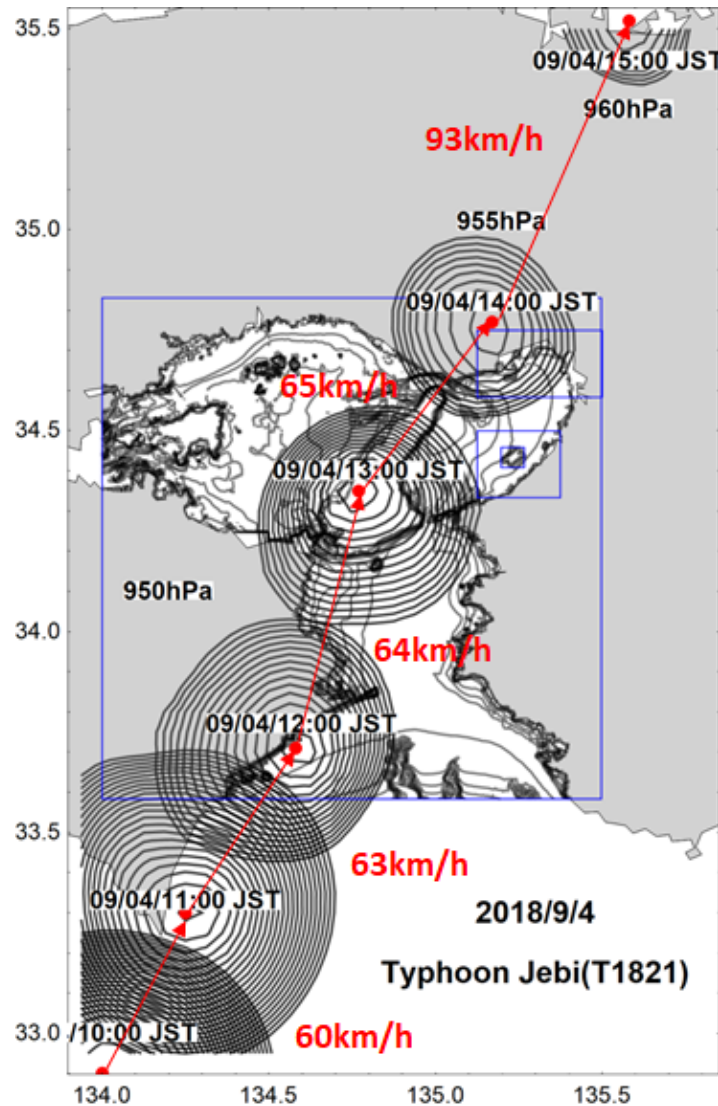

Fig. 5. The tracking of Typhoon Jebi.

3.2 Modification of wind field

This rapid acceleration of the typhoon moving speed around 13:40 is thought to be caused by the upper air westerly jet, but this phenomenon is not reflected in JMA GPV surface wind that is updated every hour. Figure 6 shows the 10-minute average wind speed observed by KIX (red line) and the 20-minute linear interpolations (blue line) of the hourly JMA GPV wind speed (orange circle). The

black line in the figure shows the time series of wind speed at the KIX observation point in the wind field modified by the method shown below. In order to introduce this short-term meteorological change into storm surge and high wave computation, it is necessary to modify the GPV wind field using two simple change methods. One is to amplify the wind speed field by multiplying the factor to match the observed value at the KIX observation point, and the other is to use the simple geostrophic model such as the Myers model to estimate the increased typhoon moving speed and add it to the GPV data. The former correction was performed by multiplying the GPV surface wind field at 14:00 by 1.35 times uniformly (the orange circle at 14:00). The latter assumes that the typhoon travel speed is 115 km/h at 14:00 (65 km/h at 13:00), and the increased moving wind speed field is computed by the geostrophic wind model, and it is added to the GPV data. In the figure, small black circles indicate wind speeds obtained by 20-minute interpolations of hourly GPV data (orange circles). In the computation, SWAN updated the wave field every 20 minutes and the surface shear stress field is calculated and passed to POM for computing storm surges. In the subsequent storm surge and wave computation, the results of the modified GPV wind data and the original JMA GPV wind data are shown in comparison.
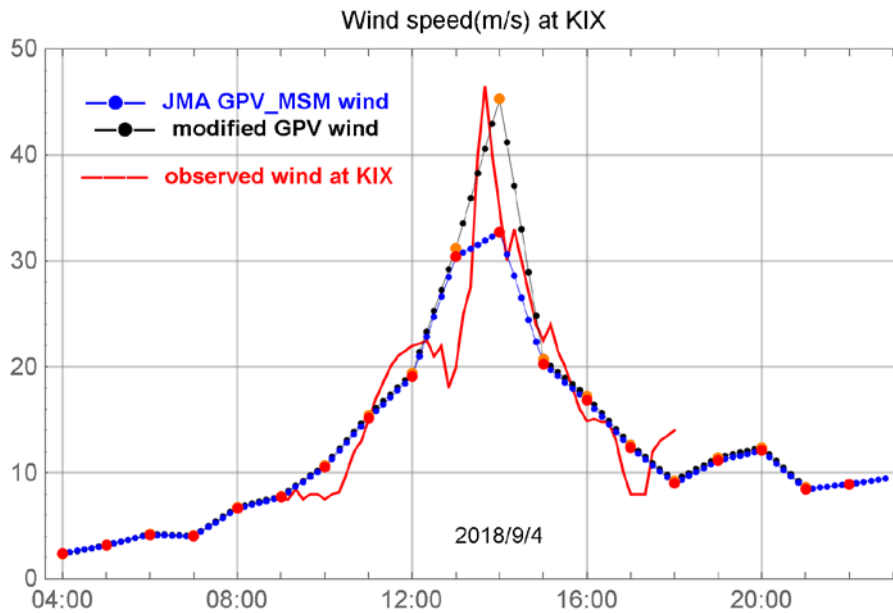
Fig. 6. The observed 10-minute average wind speed at KIX (red line) and linear interpolation of hourly JMA GPV surface winds (blue line).

Figure 7 shows the spatial distribution of the maximum wind speed during the analysis period in which (a) shows the uniform enhancement of surface wind speed, (b) original JMA GPV wind, and (c) addition of the increased typhoon moving speed (from 65 km/h to 115 km/h) to the GPV data. The modified wind field (a) and (c) seems to be able to reproduce the maximum average wind speed of 46.5 m/s observed at KIX. Figure 7 shows that the strong wind region is reproduced at the northern end of Osaka Bay by modification of the GPV wind. In the following computation, the uniform enhancement of GPV surface wind speed at 14:00 was used because of no significant difference between (a) and (c).

(a) Uniform enhancement of surface wind field

(b) Original JMA GPV

(c) Add the increased typhoon moving speed to original GPV data
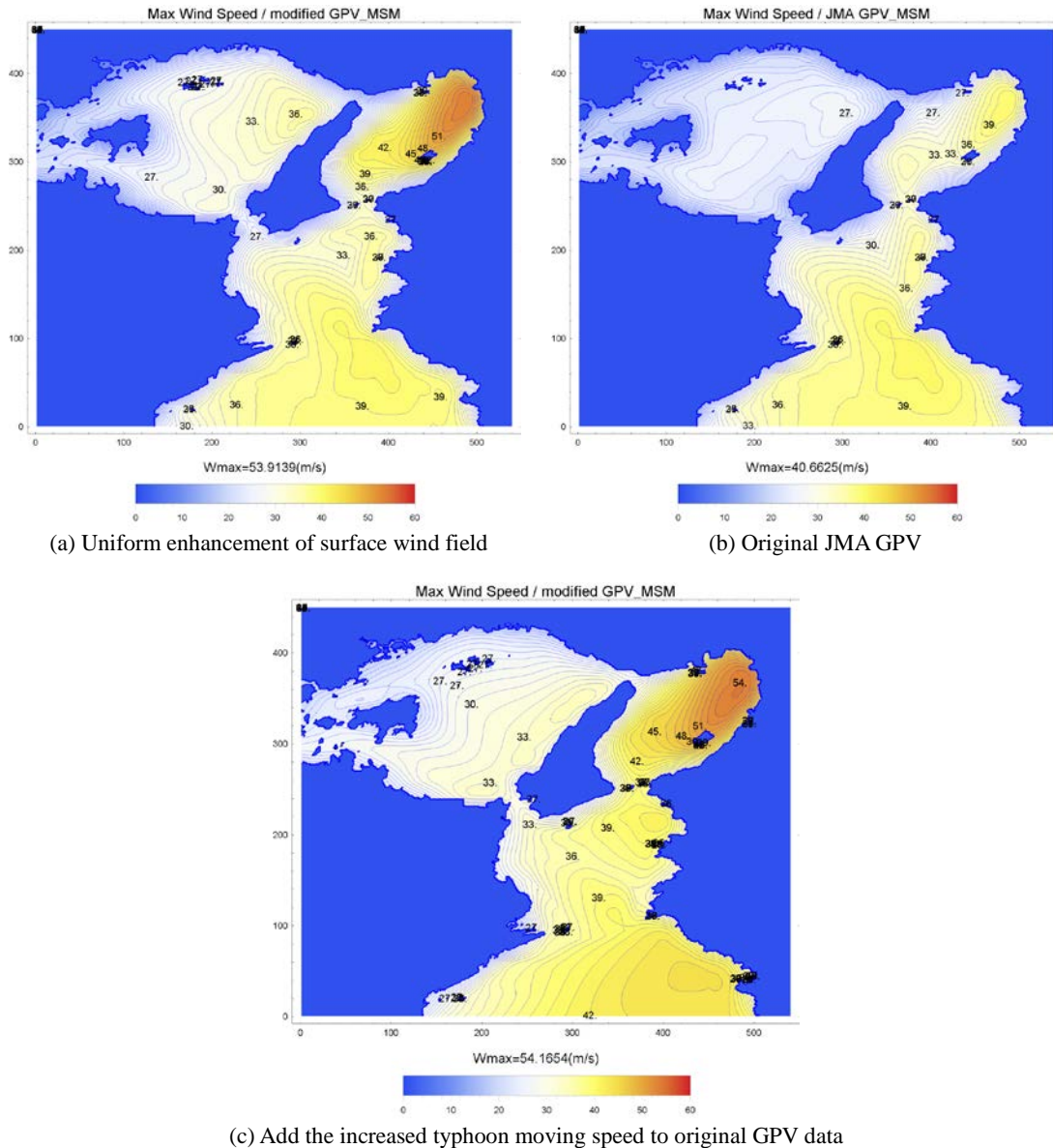
Fig. 7. Spatial distribution of the maximum surface wind speed of Typhoon
Jebi for 3 cases of wind field, uniform enhancement, original JMA GPV,
and consideration of the increased typhoon moving speed.

## 4. REPRODUCTION OF STORM SURGES AND WAVES IN OSAKA BAY SYSTEM

4.1 Significant wave height

Wave analysis is conducted with SWAN using third-generation model physics GEN3, Westhuysen,
that used nonlinear saturation-based white capping combined with wind input. On the south boundary
of Osaka Bay Domain, the offshore wave boundary (wave height, period, and wave direction) was
imposed by the observed values of the 20-minute intervals of NOWPHAS GPS wave gauge data of the
off Tokushima Kaiyo (the wave information network in Japan, 2019).

For wave direction and period, some corrections were performed with reference to the 3-hour
interval reanalysis dataset of NOAA WW3, (Wave Watch III data access site of the National Oceanic
and Atmospheric Administration, USA). (ftp://polar.ncep.noaa.gov/pub/history/waves)

Figure 8 shows the distribution of the maximum significant wave height computed by SWAN

using the modified GPV surface wind (left figure) and the original GPV wind (right figure). The difference by the wind field modification is remarkable in the north of Osaka Bay where the maximum wave height reached 4.5 m in the simulation. The authorized maximum significant wave height of 4.75 m off Kobe Airport at 14:20 on Sep. 4th was not reproduced. (From the "Report on verification of Typhoon Jebi damage" of the Kinki Regional Development Bureau (MLIT) (2018))
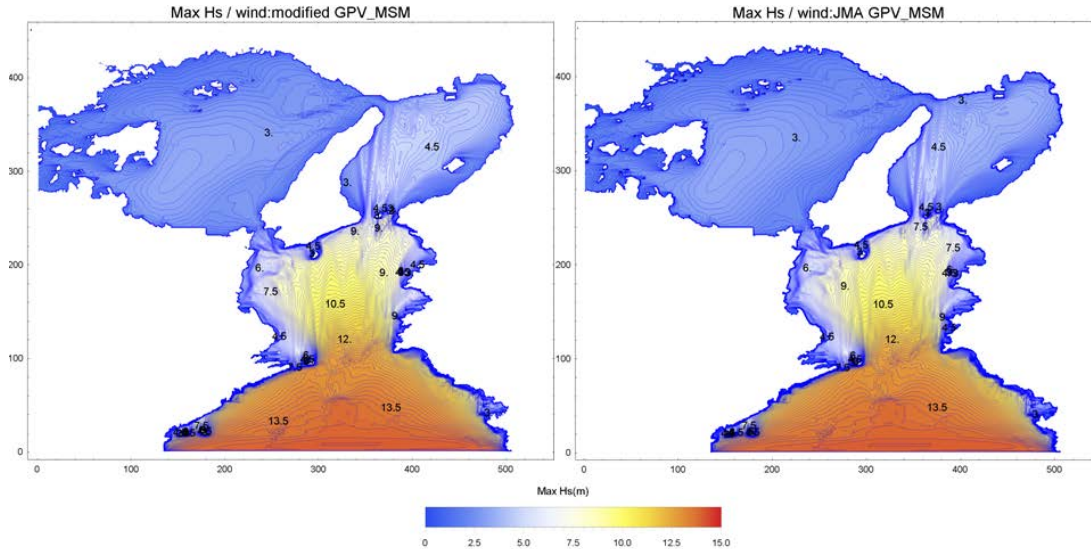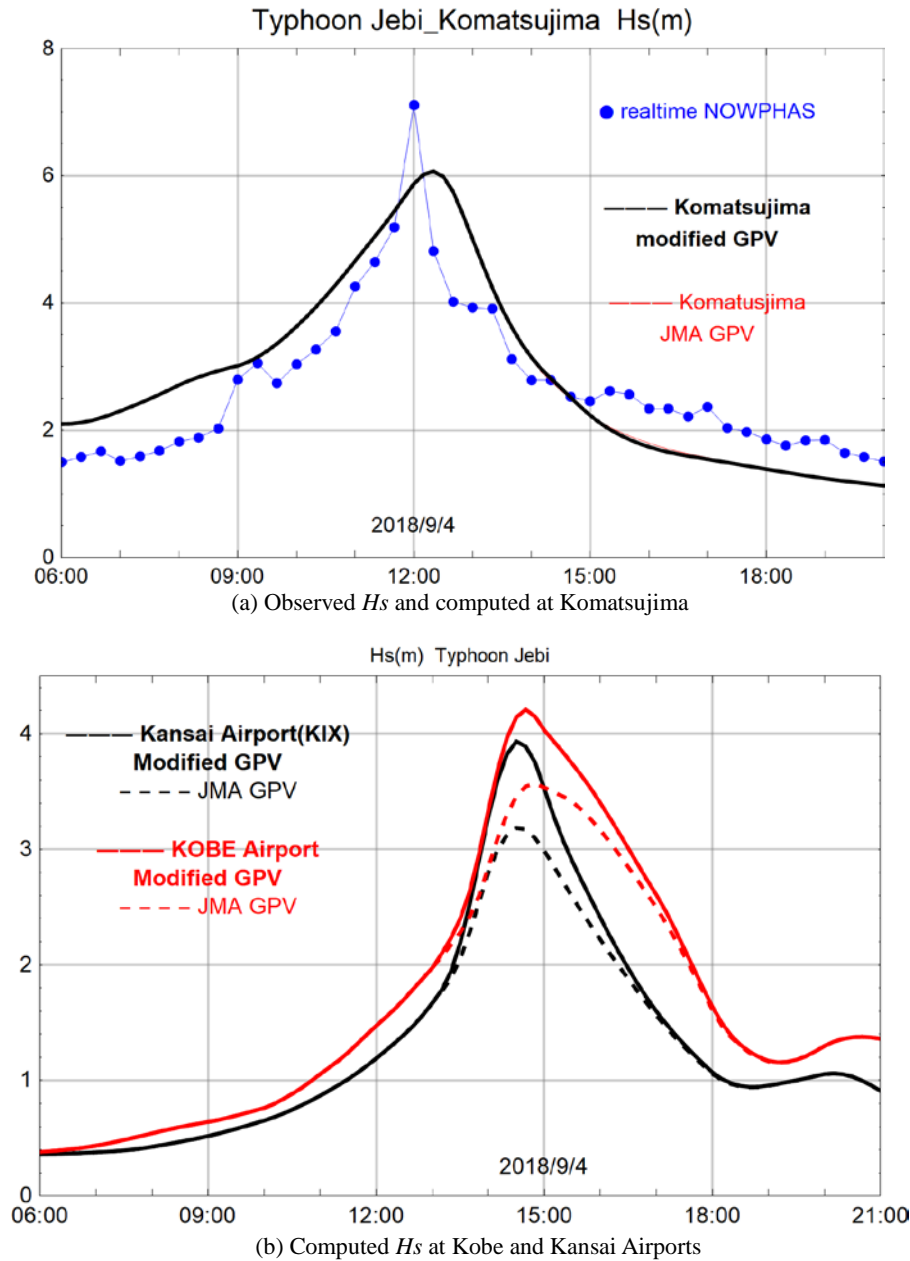

Fig. 8. The maximum significant wave height distribution computed by SWAN using the modified GPV surface wind (left) and the original GPV surface wind (right).

Figure 9 shows real-time NOWPHAS data (blue line) and SWAN computation off Kobe. The red line in the figure is the result off Kobe Airport, the black line is the result off Rokko Island, the dashed line is the result from JMA GPV wind data, and the medium line is the result from modified GPV wind. In NOWPHAS real-time data, a significant wave height of more than 8 m was observed, but this is a measurement error, and the official observations corrected later are indicated by red circles. The maximum observed significant wave height off Kobe corrected by the pressure wave gauge measurement is announced as 4.75 m.
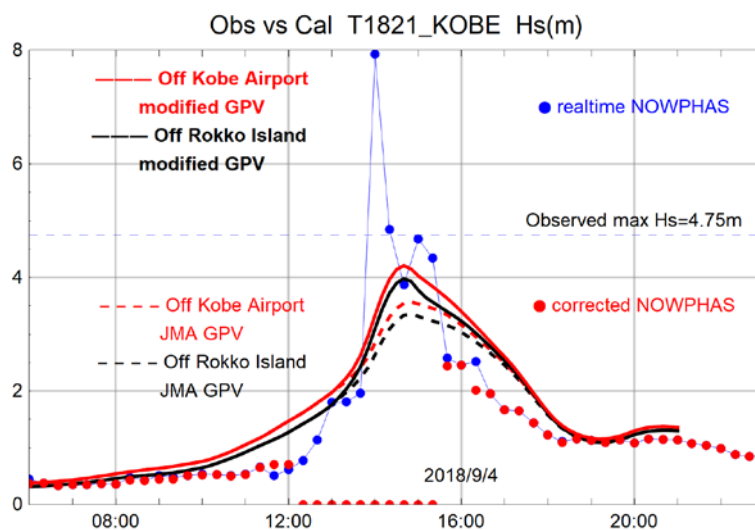
Fig. 9. Significant wave heights off Kobe coast. NOWPHAS real time observation (blue line) and corrected data (red circles). SWAN computation off Kobe Airport (red line) and off Rokko Island (black line).

53

Figure 10(a) shows the comparison between the observed (blue circles) and computed (black and red lines) significant wave heights, Hs, at Komatsujima in the Kii Channel where there is quite a small difference in the computed results by the original and modified GPV wind fields. The figure indicates that the computed wave height rises earlier than that observed. Figure 10(b) shows the computed results off Kobe Airport and Kansai International Airport (KIX) where the bold line is the results by modified GPV wind, and the dashed line by the original JMA GPV wind. The computed significant wave heights off KIX are 3.2 m and 3.9 m for the original and corrected wind fields, respectively. Those at Kobe Airport are 3.6 m and 4.3 m.


(a) Observed *Hs* and computed at Komatsujima

(b) Computed *Hs* at Kobe and Kansai Airports

**Fig. 10**. Time series of significant wave height at Komatsujima and two airport islands.

4.2 Storm surge anomaly

Figures 11 and 12 show the spatial distribution of the maximum value of the computed storm surge anomalies in Osaka Bay Domain in contour (left) and bird's eye view (right). Figure 11 shows the

results by the modified wind field, and Figure 12 shows the results by original JMA GPV wind. The local high anomalies along the coast in the Kii Channel are the wave setup inside the surf zone. This is called the "wave setup storm surge" (Washida et al., 2019). This wave setup storm surge cannot be reproduced without taking into account the surf zone dynamics analyzed by the radiation stress gradient or breaking wave stress. The vertical axis of the bird's eye view is standardized at a height of 3.0 m. The difference between the maximum storm surge anomaly calculated by the two wind speed fields (original and modified) is particularly remarkable at the northern end of Osaka Bay. The maximum storm surge anomaly calculated by the modified wind field is more than 2.8 m, but the maximum anomaly by the original JMA GPV wind field is about 2.4 m at the end of the bay.
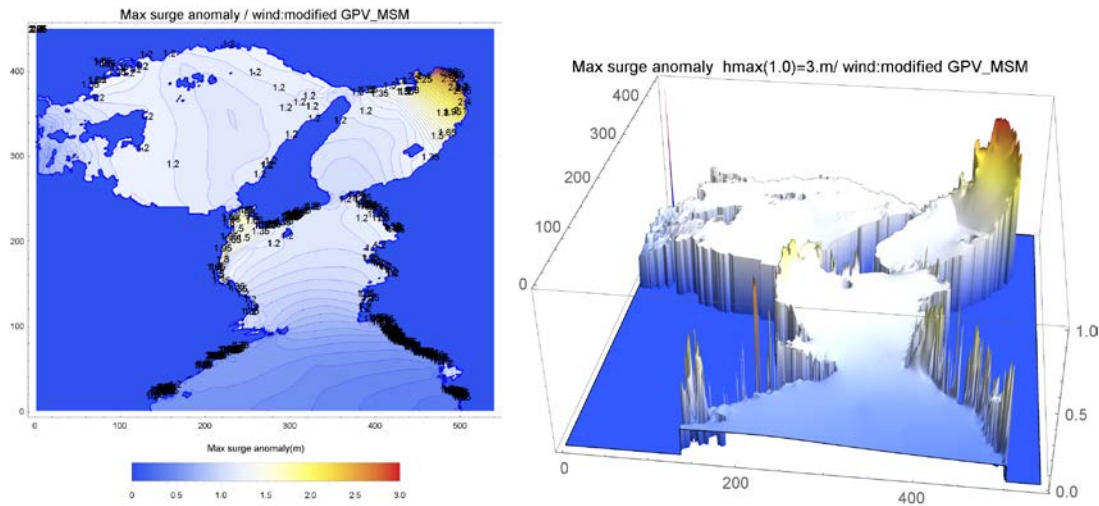
Fig. 11. The spatial distribution of the maximum computed storm surge anomalies in Osaka Bay Domain where the modified GPV surface wind was used.
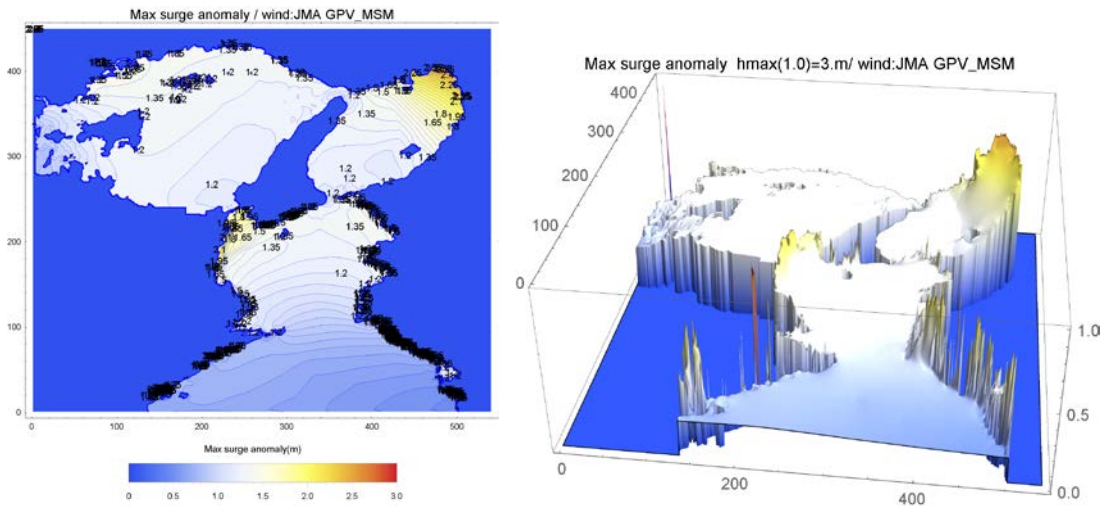
Fig. 12. The spatial distribution of the maximum computed storm surge anomalies in Osaka Bay Domain where the original JMA GPV surface wind was used.

(a) Port of Osaka

(b) Port of Kobe
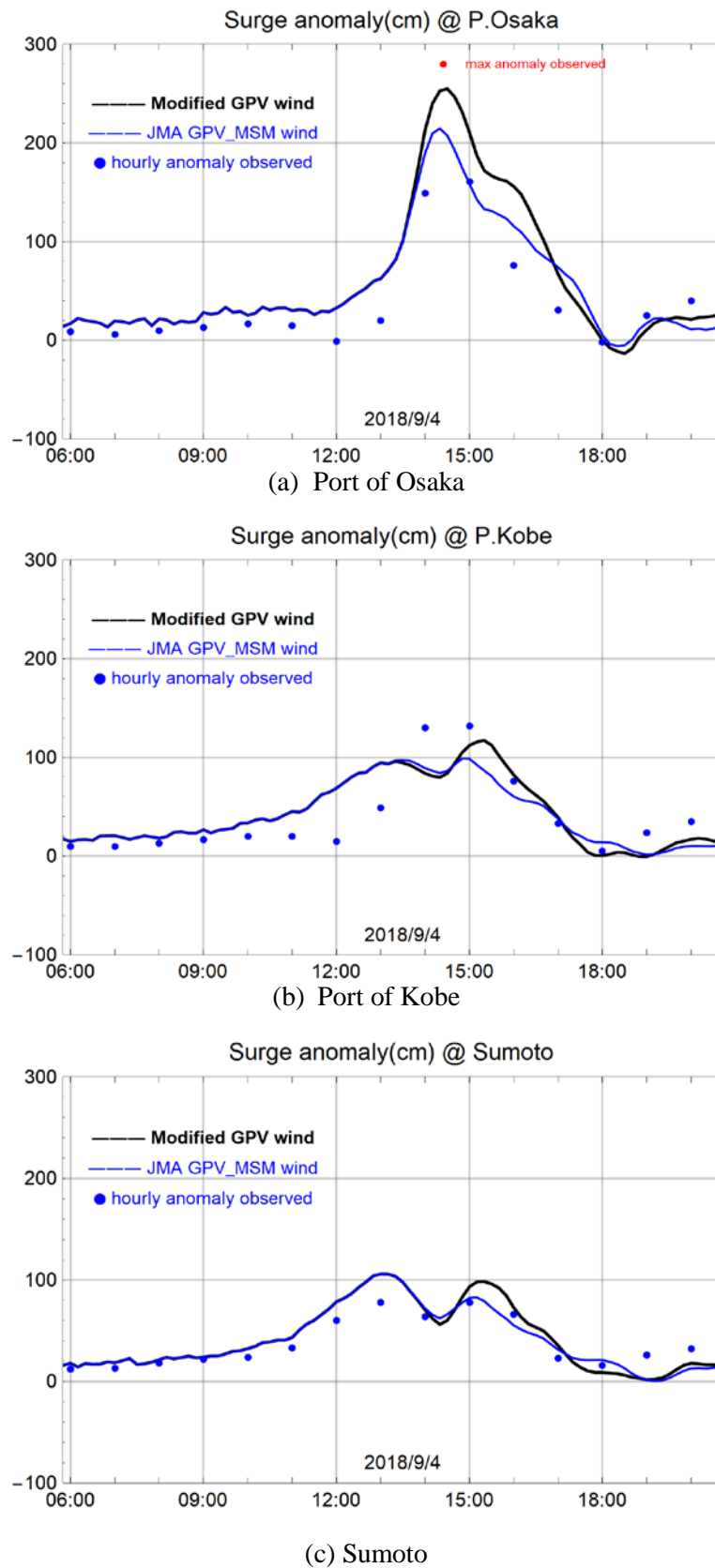
(c) Sumoto

Fig. 13. Observed (blue circles) and computed storm surge anomalies at Port of Osaka, Port of Kobe, and Sumoto.

Figure 13 shows the observed (blue circles) and the computed (lines) storm surge anomalies at the Port of Osaka, Port of Kobe, and Sumoto in Osaka Bay Domain. The maximum storm surge anomaly of 2.77 m observed at the Port of Osaka is indicated by a red circle. The maximum anomaly computed by the modified wind field (black line) is about 2.6 m. This large difference may explain why the local amplification effect due to topography is not taken into account by a course horizontal resolution of 250 m mesh in Osaka Bay Domain. Comparing the observed and computed time series of storm surge anomalies at three stations, it is clear that the computed result tends to rise more quickly. This is the same tendency as significant wave heights simulation in which the computed wave height rises earlier than the observed wave height. The difference between this computation and the observation may depend on the boundary conditions and wind field differences in wave analysis.

5. SURGE AND WAVES IN HANSHIN PORTS AND YODO RIVER MOUTH

In the northern part of Osaka Bay, inundation disasters due to overtopping and overflowing in the artificial islands occurred in many places in the Port of Kobe area and a storm surge anomaly exceeding O.P.+5.2 m, (T.P.+3.9 m) downstream of Yodo River was recorded. In order to elucidate this mechanism of these abnormal water level and inundation disasters, a detailed analysis was conducted in Hanshin Port and Yodo River mouth using 50 m mesh resolution nesting from Osaka Bay Domain (250 m mesh). The nesting of wave analysis was performed by SWAN code and the nesting of current analysis was done by passing the water level boundary condition in POM computation.

5.1 Significant wave height
Figure 14 shows the spatial distribution of the maximum significant wave height in the Hanshin Port area computed by modified wind field. The output points off Rokko Island and Kobe Airport are indicated by red circles.
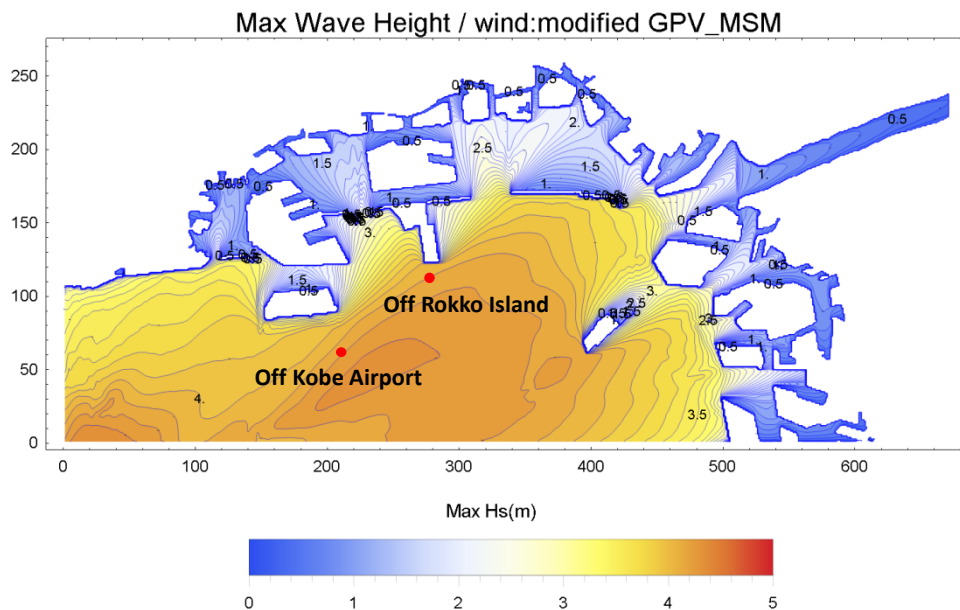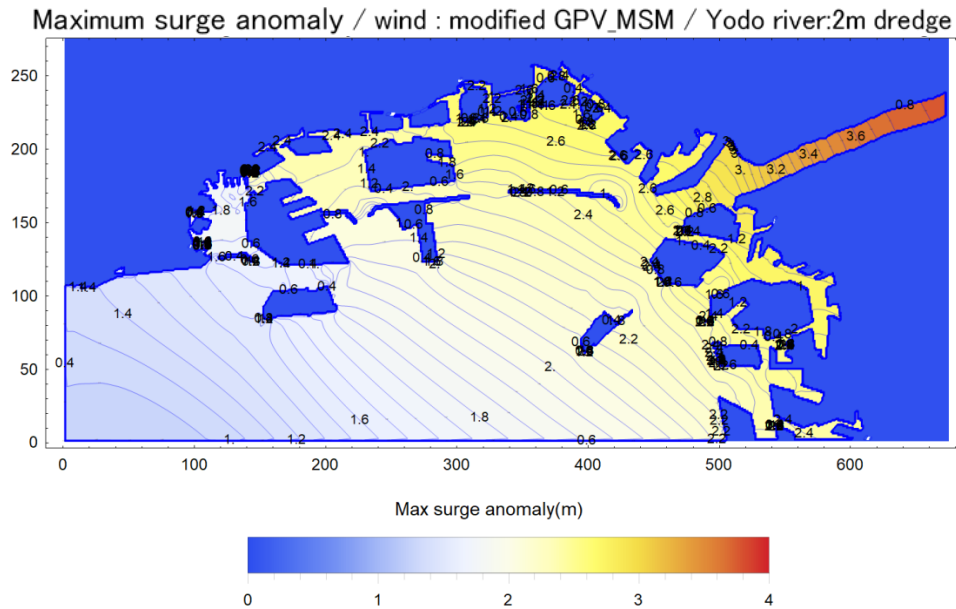

Fig. 14. The spatial distribution of the maximum significant wave height in the Hanshin Port region.

The offshore breakwater that protects the Port of Kobe from high waves seems to be functioning, but the invasion of waves from the opening cannot be ignored in the east part of Rokko Island. In Osaka Port, the coastal area is protected from high waves by offshore artificial islands.

Because high waves strike the offshore artificial islands directly, a higher design crown height is necessary in this area.

5.2 Storm surge anomaly

The spatial distribution of the maximum storm surge anomaly in the Hanshin Port area is shown in Figure 15. Since there is no data in the port area in the digital chart M7000 series, the water depth behind the offshore breakwater is assumed to be uniformly 8.85 m (MSL or higher).


Fig. 15. The spatial distribution of the maximum storm surge anomaly in the Hanshin Port region.

For this reason, it is necessary to consider the possibility that there is a slight error in the reproduction accuracy of the storm surge anomaly in the port area. Similarly, the water depth in the Yodo River is also set uniformly at 2.88 m (above MSL), so note that the computed storm surge anomalies here do not have high reliability.

Although not confirmed by analysis, the storm surge control effect of the offshore breakwater at the Port of Kobe seems to be weak. Furthermore, it is necessary to note that the storm surge stay period may be lengthened to prevent the seawater accumulated inside the offshore breakwater from flowing out due to longer breakwaters. The maximum storm surge anomaly in the Yodo River is reproduced as M.S.L.+3.8 m (O.P.+5.2 m), which is consistent with the observation results.

Figure 16 shows snapshots of the current velocities and storm surge anomalies at 14:20 and 14:40 when the tide level is supposed to have reached its maximum. In this phase, the water level rises but the flow velocity is weak. A strong westward flow is seen between Rokko Island and the offshore breakwater.

Figure 17 shows output points of the storm surge anomaly (upper) and the time series of the storm surge anomaly (lower). The lower left figure shows the result using the modified wind field, and the right shows the result by original JMA GPV_MSM surface winds. The maximum anomalies above MSL at each output point are shown in meters. According to the report of the Kinki Regional Development Bureau (2018), MLIT, Japan, the observed anomalies at the Port of Osaka are 2.77 m, 2.72 m at Nishinomiya, 1.81 m at the Port of Kobe, and 3.85 m upstream of the river, respectively. These values correspond with the results computed by the modified wind field (lower left figure).
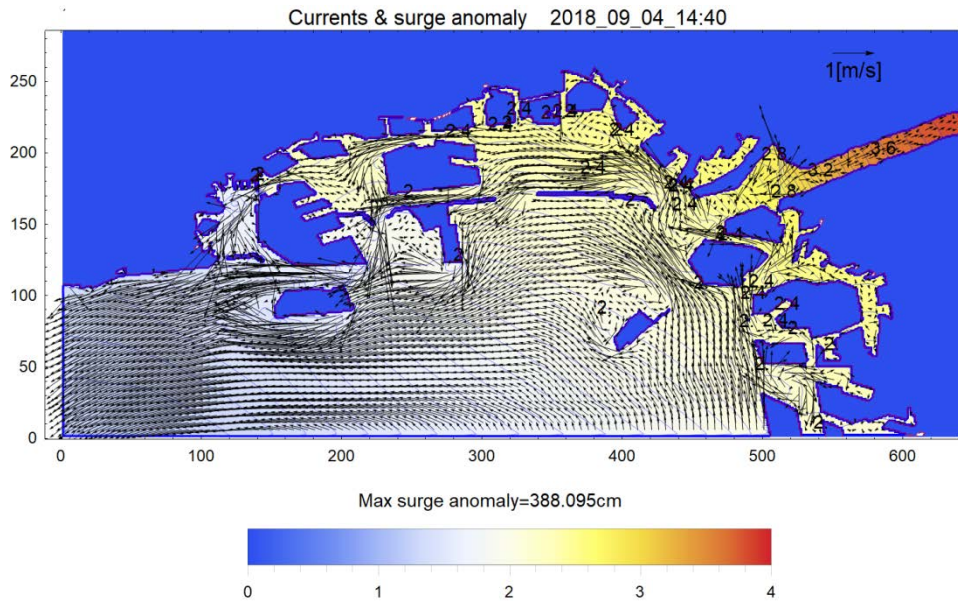
Fig. 16. Snapshots of the current velocities and storm surge anomalies at 14:40.

5.3 Storm surge in Yodo River mouth

In order to establish countermeasures against storm surges in the Yodo River estuary and determine the design crown height of coastal revetments and river dikes, detailed numerical analysis of estuary storm surges using accurate topographic data of river channels is necessary. In the river estuary and channel, storm surge and tsunami rapidly increase the height. If this increase cannot be dealt with by raising the river dike alone, a dredging of the river channel can be considered as an alternative. In this computation, we analyzed the degree of effect that can be expected when dredging 2.0 m uniformly in the river channel. Since there is no detailed information on Yodo River channel topography, the river mouth storm surge was analyzed assuming the depth to be M.S.L.-2.88 m.

When the river storm surge amplification phenomenon cannot be dealt with just by raising the river bank, as an alternative method, river channel dredging is a possibility. We analyzed what effect can be expected if uniform 2.0 m dredging in the river channel is conducted.

Figure 18 shows the difference (in cm) of maximum storm surge anomalies before and after the river channel dredging. This figure shows that a 2.0 m river channel dredging can suppress the rise of the water level in the river channel by up to 12 cm, but the water level has increased by 14 cm in the estuary. If the dredged material can be utilized for reclamation of the offshore artificial islands, it is worth conducting a detailed analysis on the storm surge reduction effects of dredging including the cost performance.

From the comparison of the river water surface profiles (shown in Figure 19) at the time of the maximum storm surge anomaly and 10 minutes before it, it is clear that the water level rise at the estuary is due to the relaxation of the river water surface gradient by the dredging. This is the mechanism of storm surge reduction by dredging and the water level rise at the estuary is much smaller than water level reduction in the river channel.

(a) Output points

(b) Modified GPV wind

(c) Original JMA GPV wind
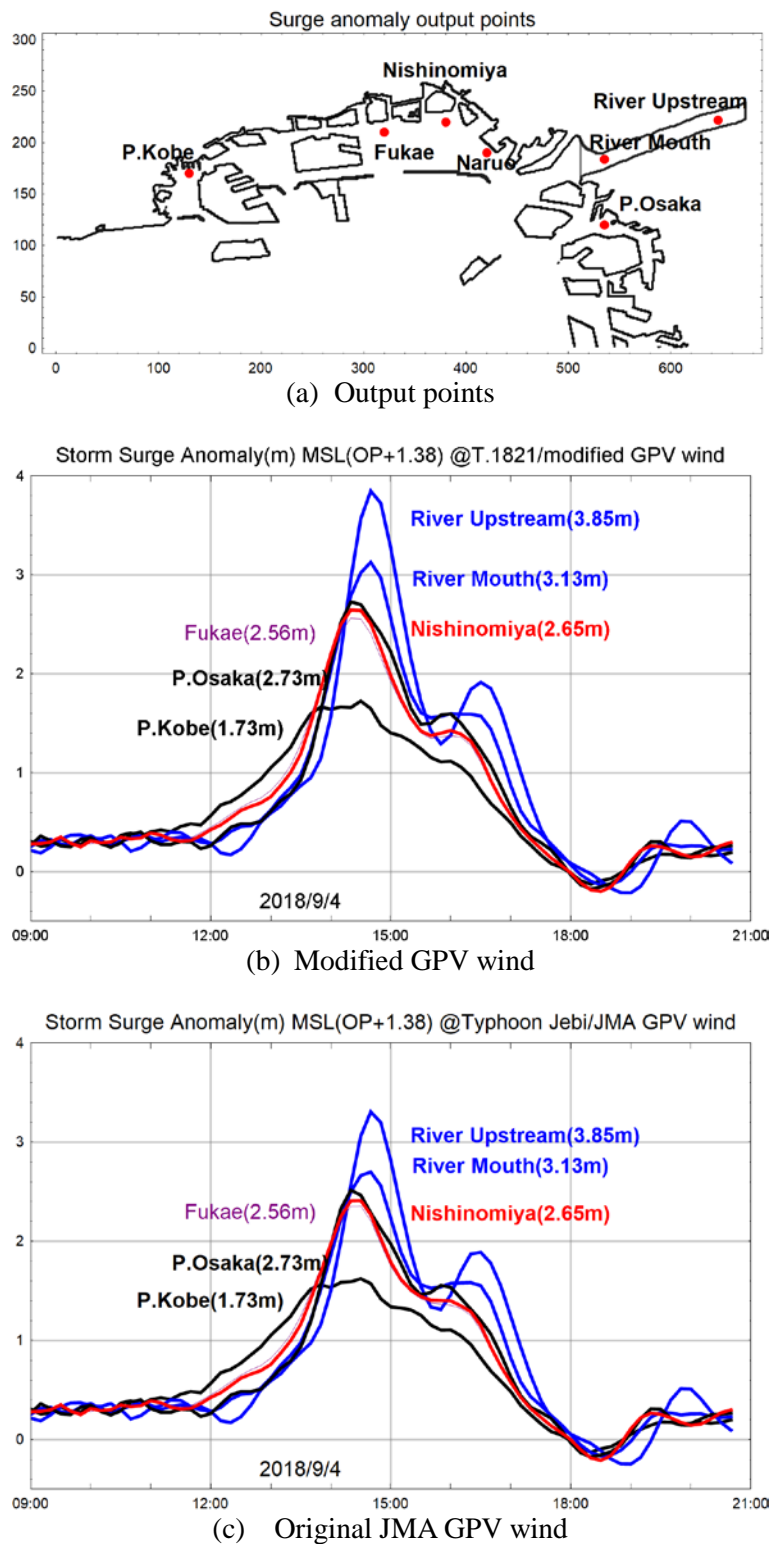
Fig. 17. Output points and the time series of the storm surge anomalies for the modified GPV wind and the original JMA GPV wind.

Dredging effects in max surge anomaly (cm)
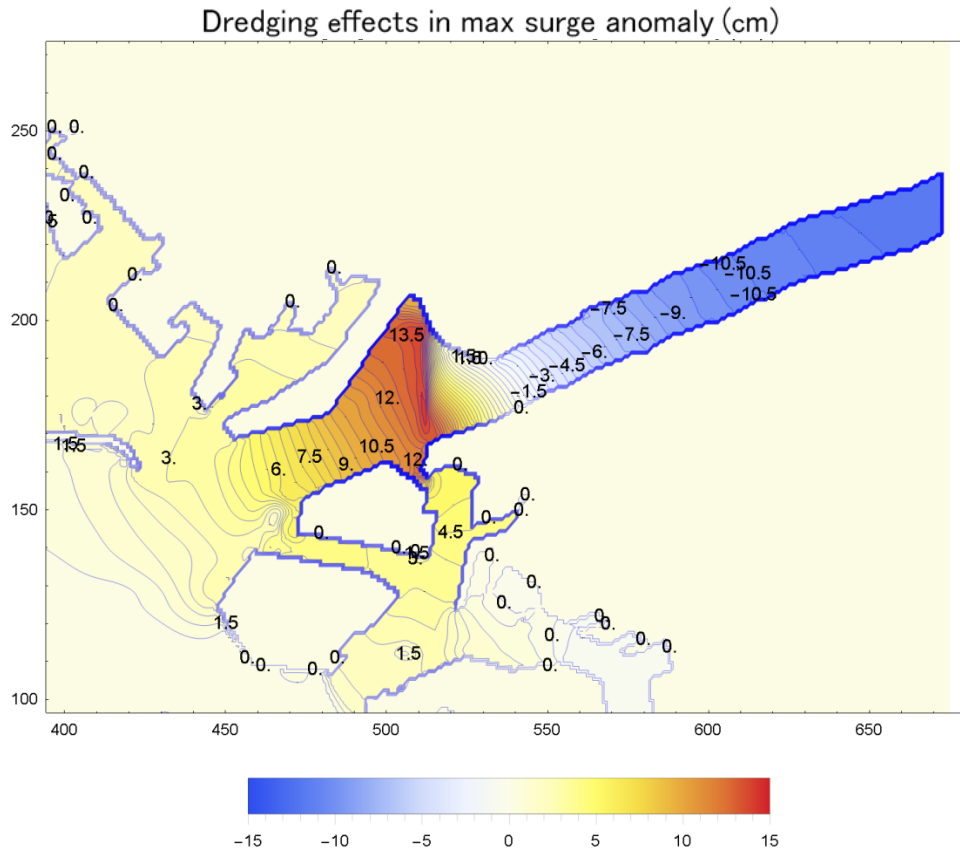
Fig. 18. The difference of the maximum storm surge anomalies before and after the dredging (in cm).

Water surface profile in Yodo River mouth (MSL)
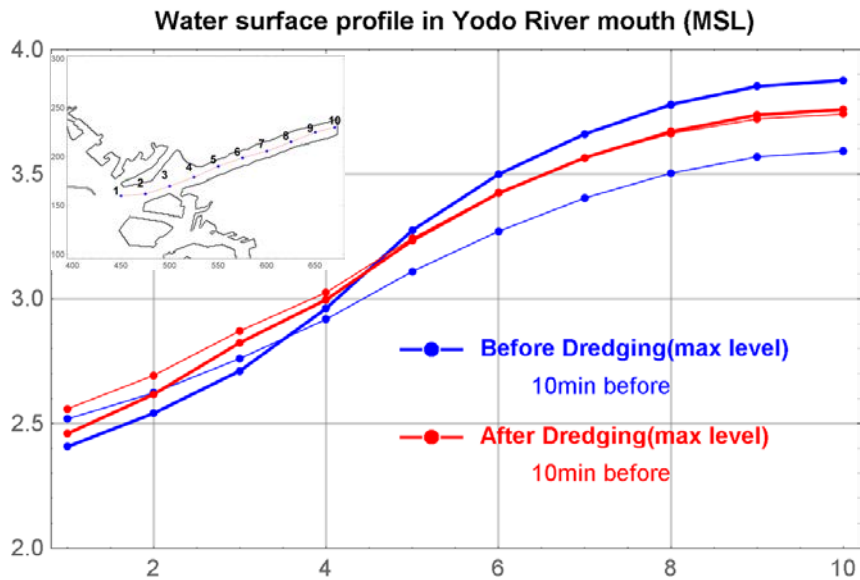
Fig. 19. The water surface profile along the river channel at the time of maximum storm surge (thick line) and 10 min before maximum (thin line).

61

## 6. STORM SURGE AND WAVES AROUND KANSAI INTERNATIONAL AIRPORT (KIX)

6.1 Significant wave height

In Typhoon Jebi, Kansai International Airport also suffered a flood disaster due to wave overtopping. According to the third party committee established by the operating company, Kansai Airport (2019), it was concluded that 90% of the flood was caused by the overtopping of the high waves striking the revetment. The committee estimated the maximum wave height off the airport island to be 5.2 m at the observation station, west side of the island by the numerical simulation conducted by the committee and pointed out that it was a huge wave that had never been observed before. However, major overtopping disasters were prominent on the southeast side of the airport island on the leeward side of waves in which the significant wave height of this study was about 2.5m. The reason why the committee did not discuss significant wave heights on the southeast side is unknown. In order to examine the mechanism of this unexpected disaster event, SWAN wave simulation was conducted in this study to confirm the wave field around the island. The results from discussion in the committee were summarized by Ito et al. (2019).

Figure 20 shows the maximum significant wave height distribution of SWAN wave simulation conducted in this study using the modified GPV wind and the original JMA GPV wind data. This figure shows that the maximum significant wave height in the southeastern region of KIX Island is about 2.5 m even in the modified wind field computation results.
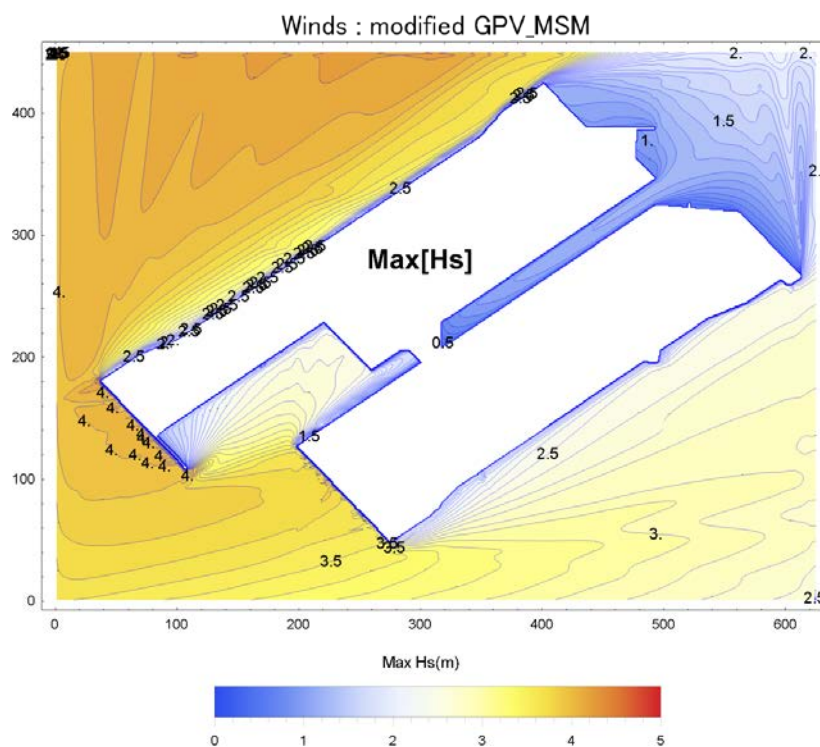
Fig. 20. The maximum significant wave height distribution
in the airport island region (modified GPV wind).
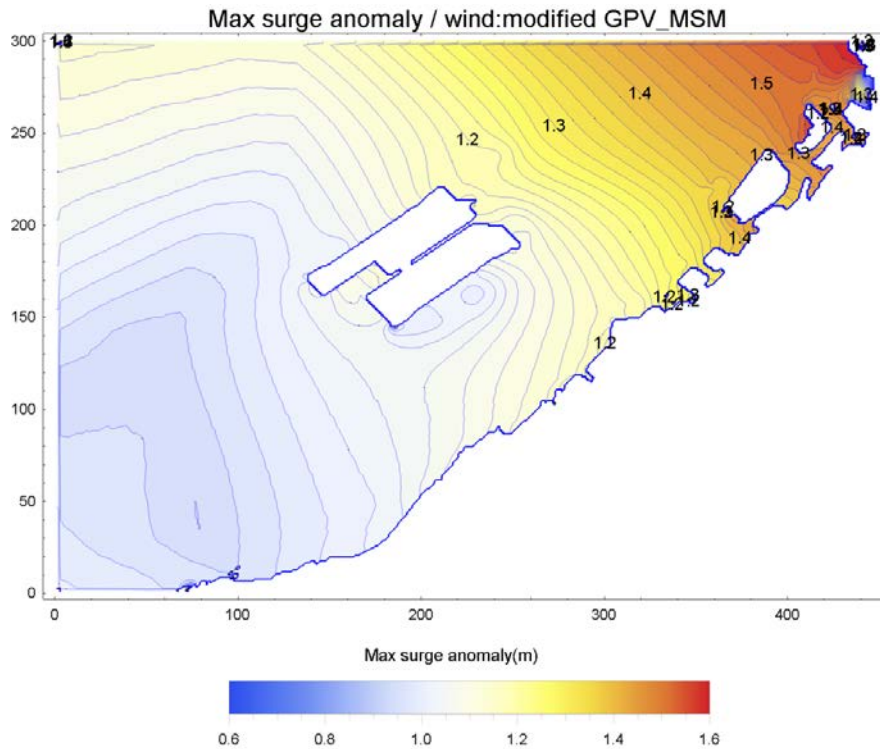
Fig. 21. The maximum storm surge anomaly distribution
around KIX (modified GPV wind).

6.2 Storm surge anomaly around airport island

In addition to examining the possibility of the occurrence of wave setup and storm surges around the airport island, storm surge analysis was conducted to confirm how much the rise in mean sea level caused by storm surges promoted overtopping disasters.
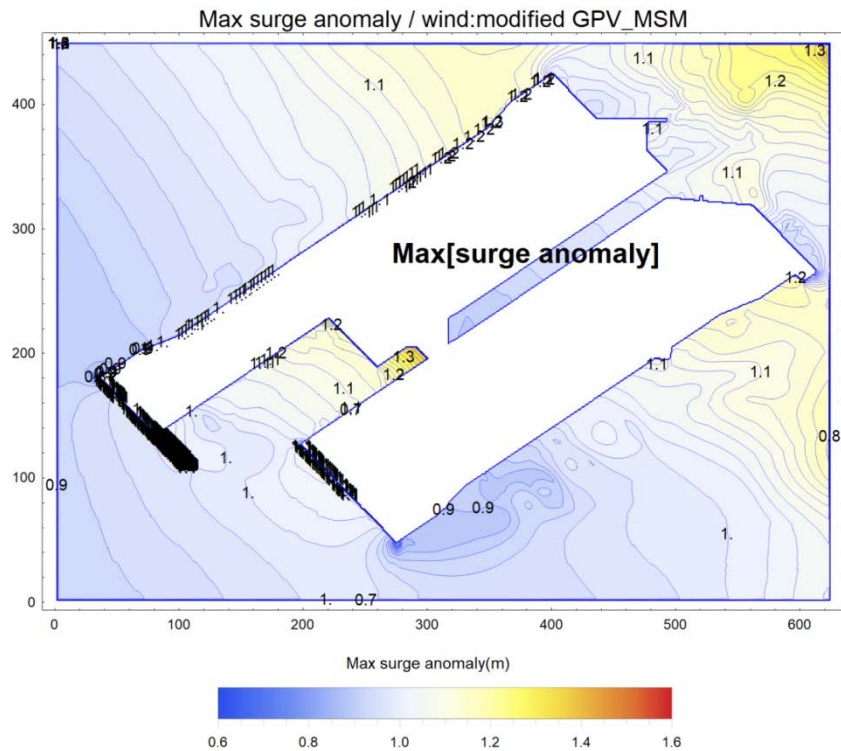
Figure 21 shows the distribution of the maximum value of the storm surge anomaly in two cases using the modified wind speed field and the original JMA GPV data. The results of the modified wind speed field show that the maximum storm surge anomaly in the southeastern part of the airport island is about 1.2 m.

The design crown high of the revetment is defined by the design high tide level (storm surge anomaly+ syzygy average high tide level) + half wave height+ margin height.

From the results of significant wave height and storm surge anomaly shown here, the following can be estimated. Half of the significant wave height of 2.5 m is M.S.L.+1.25 m, the tide level in Osaka Bay at the time of the maximum storm surge is M.S.L.+0.22 m, and the maximum storm surge anomaly around the airport island is M.S.L.+1.2 m. From the total, the maximum water level generated by the typhoon on the southeast side of the airport island is estimated to be M.S.L.+2.67 m. For M.S.L. = C.D.L.+0.95 m, the maximum water level from the chart datum level is C.D.L.+3.62 m.

If the sum of the maximum water level and the margin height is higher than the actual height of the revetment, overtopping and overflowing disasters may occur. According to data by Kansai Airport (2019), the current height of the southeast bank of the airport island is C.D.L.+3.9 m. If the margin height is 0.54 m (assuming 20% of the estimated maximum water level 2.67 m), the water level as an external force is C.D.L.+4.12 (= 3.62+0.54) m. The exact margin height setting and an analysis of wave overtopping discharge are necessary to confirm the mechanism of inundation disaster of Kansai Airport.

Figure 22 shows the maximum storm surge anomaly in the second nesting KIX computational domain (10 m mesh). The wave setup storm surge around the airport island was not reproduced in the simulation and the storm surge anomaly was high in the northwestern part of the island.

Fig. 22. The maximum storm surge anomaly distribution
in the airport island region (modified GPV wind)

Figure 23 is a snapshot of the storm surge anomaly and the spatial distribution of the mean current at the time when the maximum storm surge occurred. The flow from the southwest is prominent, and a strong current is formed between the airport island and the land. A tanker anchored off the southwestern part of the airport island was swept away by a strong wind and collided with the connecting bridge. It is understood that the southwest current mentioned here may have caused the tanker to drift from the anchoring point to the end of the connecting bridge.
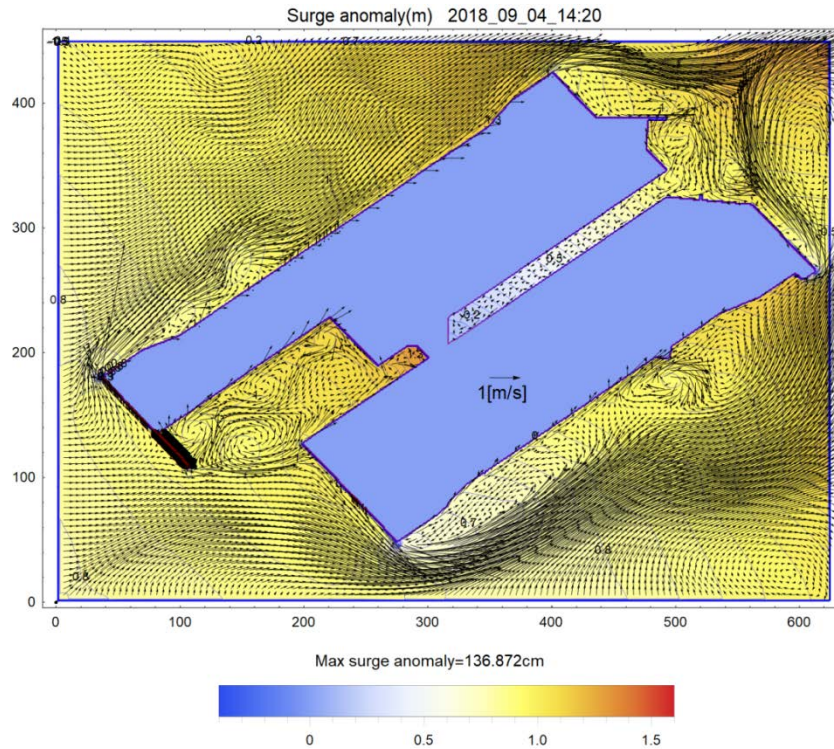
Fig. 23. Snapshots of the storm surge anomaly and the ocean current (modified GPV wind).

6.3 Wave-surge combined height distribution in the north end of Osaka Bay

Assuming that a large-scale inundation occurs mainly in the zero-meter zone along the coast of Osaka Bay due to extreme storm surges, the measures for protecting human lives, avoiding impacts on the central functions of cities, social and economic functions, and focusing on early recovery, should be considered in advance by the related organizations. For this purpose, the Osaka Bay Storm Surge Countermeasures Council was established by the Kinki Regional Development Bureau at the Ministry of Land, Infrastructure, Transport and Tourism (MLIT). This council held a conference on "Current status and challenges for storm surge in Osaka Bay", in which Reference document 1 of the First meeting (held on July 11, 2007) was distributed. Its sources are Kobe City materials, Hyogo prefecture materials, Osaka City materials, Osaka Prefecture materials, and "Osaka Bay Alongshore Coastal Conservation Basic Plan" (Osaka Prefecture, Hyogo prefecture). For document 1, refer to the URL of the Kinki Regional Development Bureau (2007), Ministry of Land, Infrastructure, Transport and Tourism (MLIT).

The design crown height along the north end of Osaka Bay shown in Figure 24(a) was cited from the Reference document 1. Figure 24(b) shows the summary of output on the computed maximum water level (surge anomaly + half of significant wave height + astronomical tide) in this study.
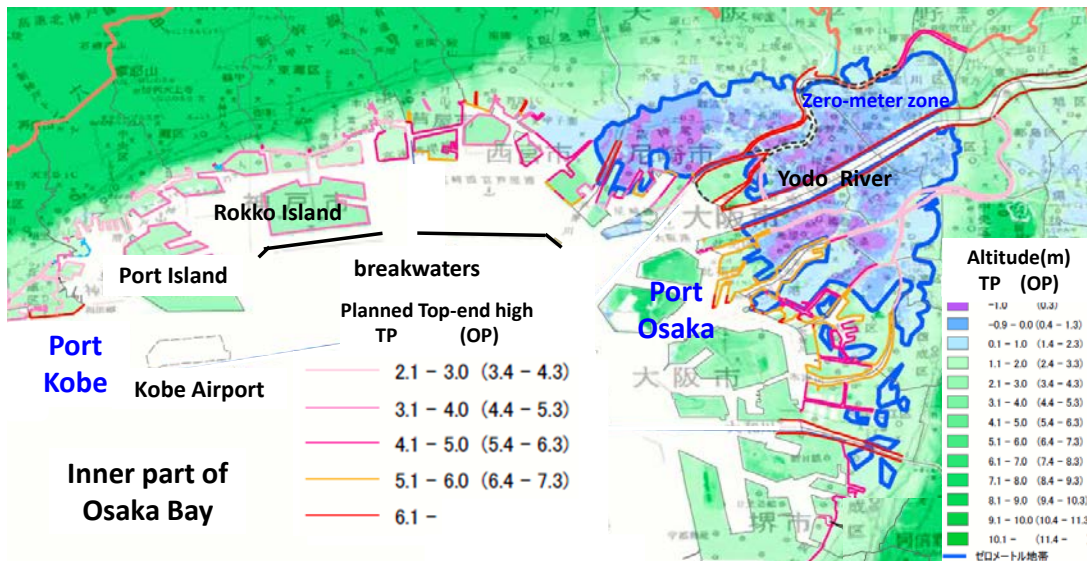
(a) The design crown height in the north end of Osaka Bay
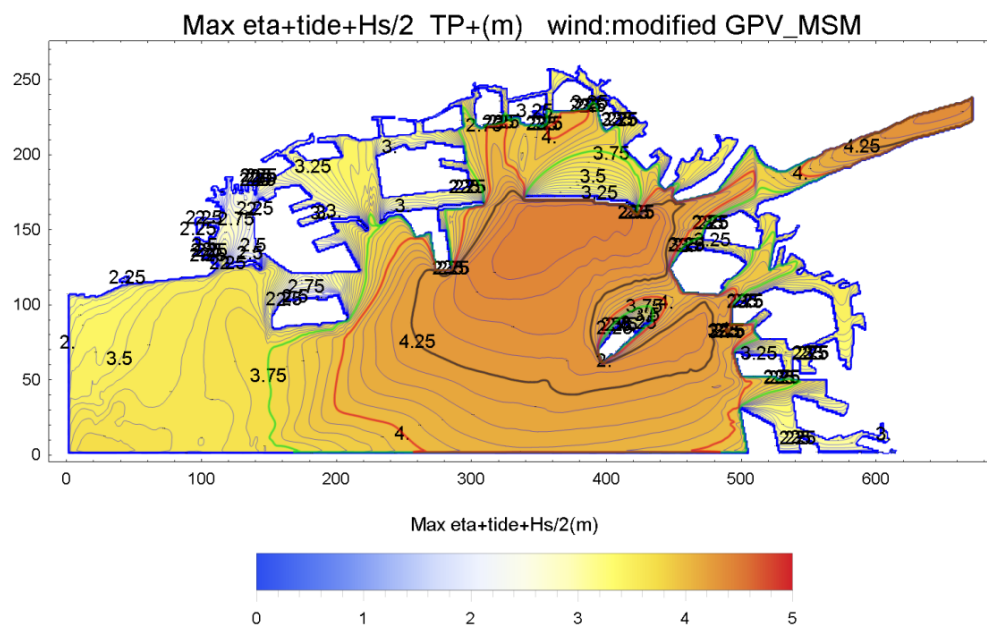
(b) Computed maximum water level (surge anomaly + half of significant wave height
+ astronomical tide)

Fig. 24. The design crown height and the computed maximum water level of Typhoon Jebi.

Comparing Figure 24 (a) and (b), the following findings were obtained about storm surge disasters caused by Typhoon Jebi.

(1) The area of the Port of Osaka is protected by offshore artificial islands. The seawall with a design crown height of T.P.+6 m or more is essential on an offshore artificial island exposed to high waves.

(2) Storm surges and tsunamis are strengthened in rivers. The prevention of storm surges at the Yodo River estuary and river channel between the two ports of Kobe Port and Osaka Port is weak due to the geographical characteristics of the management system by different prefectures. The disaster prevention function that only strengthens the river bank is insufficient, and new prevention measures are necessary.

7. CONCLUSIONS

The fact that a large disaster occurred due to Typhoon Jebi that was much weaker than Second Muroto Typhoon confirms that the recent coastal development has not achieved the required disaster prevention measures. Typhoon Jebi was a high-speed moving typhoon and its moving speed accelerated near the end of Osaka Bay resulting in the enhancement of storm surges by the sudden increase of surface wind speed. To predict possible storm surges, not only the central pressure, but also the moving speed are important factors.

The major findings of the study are summarized as follows:

(1) The wave-surge combined numerical model used reproduced the phenomenon that Typhoon Jebi caused a storm surge anomaly exceeding 2.77m in the north end of Osaka Bay and it was mainly caused by the sudden increase of surface winds due to the acceleration of the typhoon's moving speed.

(2) The storm surge in the Yodo River channel exceeding O.P.+5.2 m was reproduced by the model. It was revealed that storm surge prevention in the Yodo River between two ports is fragile.

(3) The computed storm surge and wave height on the southeast side of Kansai International Airport Island exceeded the current crown height of C.D.L.+3.9 m which was not adequate to prevent the inundation disaster due to storm surge and high waves caused by Typhoon Jebi.

REFERENCES

1) Battjes, J.A. and J.P.F.M. Janssen: Energy loss and set-up due to breaking of random waves, Proc. 16th Int. Conf. Coastal Engineering, ASCE, 569-587, 1978.

2) Blumberg, A.F. and G.L. Mellor, "A Coastal Ocean Numerical Model", Mathematical Modelling of Estuarine Physics, Proceedings of an International Symposium, Hamburg, August 24-26, 1978. J. Sundermann and K.P. Holz, Eds., Springer-Verlag, Berlin, 1980.

3) Blumberg, A. F. and G. L. Mellor: A description of a three-dimensional coastal ocean circulation model, in Three-Dimensional Coastal Ocean Models, Coastal and Estuarine Sciences, Vol. 4, Editor N. Heap, American Geophysical Union, Washing, D.C., 1-16, 1987.

4) Ito, K., Katagi, K., Mizukami, I. and Kumagai, K.: Inundation factor by typhoon 201821 at Kansai International Airport and reproduction of inundation status, Journal of Japan Society of Civil Engineers, B2(Coastal Engineering),Vl.75, No.2, I_307-I_312., 2019.

5) Japan Meteorological Agency: Report of meteorological cases of Typhoon Jebi caused storms and storm surges, September 11, 2018.

6) Kansai Airport: Report on "Reconstruction of sea conditions and flooding" by Typhoon 21, The wave overtopping etc. verification committee, (in Japanese), April 17, 2019.

7) Kinki Regional Development Bureau, Ministry of Land, Infrastructure, Transport and Tourism (MLIT): Current status and challenges for storm surge in Osaka Bay, (in Japanese), https://www.kkr.mlit.go.jp/bousai/link/takashio/conference/qgl8vl000000dhny-att/reference _01.pdf, July 11, 2007.

8) Kinki Regional Development Bureau, Ministry of Land, Infrastructure, Transport and Tourism (MLIT): Report on verification of typhoon Jebi damage, (in Japanese), http://www.pa.kkr.mlit.go.jp/pdf/takasiotaisaku/20181218/5.pdf, December 18, 2018.

9) NOAA WAVEWATCH III: NWW3 Data Access through ftp://polar.ncep.noaa.gov/pub/history/waves, April 26, 2019.

10) Nationwide Ocean Wave information network for Ports and HArbourS (NOWPHAS), the wave information network in Japan, conducted by Ports and Harbours Bureau, Ministry of Land, Infrastructure, Transport, and Tourism (MLIT), http://www.mlit.go.jp/kowan/nowphas/index.html, 2019.

11) Princeton Ocean Model (POM) in ECOMSED: Users' Manual of ECOMSED Version 1.3, HydroQual, Inc., 2002, 188p.

12) SWAN Cycle III Version 41.01: a copy of the license is available at, https://www.tudelft.nl/en/ceg/about-the-faculty/departments/hydraulic-engineering/sections/environmental-fluid-mechanics/research/swan/, 2014.

13) Washida, M., Muroi, N. and Takahashi, T.: Numerical analysis of typhoon-induced wave setup surges along west coast of Sagami Bay, Journal of Japan Society of Civil Engineers, Ser. B3 (Ocean Development), Vol. 75, No. 2, pp.I_61-I_66., 2019.

14) Yan, L.: An improved wind input source term for third generation ocean wave modelling, Scientific report WR-No 87-8, De Bilt, The Netherlands, 1987.